

Enhancing Plausibility Evaluation for Generated Designs with Denoising Autoencoder

Jiajie Fan^{1,2}, Amal Trigui¹, Thomas Bäck², and Hao Wang²

¹ BMW Group, Bremer Str. 6, 80788 Munich, Germany
{jiajie.fan, amal.trigui}@bmw.de

² LIACS, Leiden University, Niels Bohrweg 1, 2333 Leiden, The Netherlands
{t.h.w.baeck,h.wang}@liacs.leidenuniv.nl

Abstract. A great interest has arisen in using Deep Generative Models (DGM) for generative design. When assessing the quality of the generated designs, human designers focus more on structural plausibility, *e.g.*, no missing component, rather than visual artifacts, *e.g.*, noises in the images. Meanwhile, commonly used metrics such as Fréchet Inception Distance (FID) may not evaluate accurately as they tend to penalize visual artifacts instead of structural implausibility. As such, FID might not be suitable to assess the performance of DGMs for a generative design task. In this work, we propose to encode the input designs with a simple Denoising Autoencoder (DAE) and measure the distribution distance in the latent space thereof. We experimentally test our DAE-based metrics with FID and other state-of-the-art metrics on three data sets: compared to FID and some more recent works, *e.g.*, $FD_{\text{DINO-V2}}$ and topology distance, DAE-based metrics can effectively detect implausible structures and are more consistent with structural inspection by human experts.

Keywords: Evaluation metric · Design Generation · Structural Plausibility

1 Introduction

Following the swift development of Deep Generative Models (DGMs) in general image generation tasks [17, 22, 26, 38], a great interest has arisen in using DGMs to enable generative design [15, 40], where DGMs are able to create innovative designs based on specific input requirements provided by users. In this particular domain, design data is responsible for representing the design object with structural and geometric patterns, which are required to be recognizable and plausible. In order to rank models during the development of generative models, recent works rely on a subjective evaluation [14, 34], where human experts apply an established set of criteria to manually assess a significant quantity of generated data. This evaluation method yields reliable results, serving as “ground truth” for model ranking, but it is time-consuming and hard to reproduce [34]. Hence, for developing DGMs for design generation, it is necessary to have an automated metric, which is able to reliably quantify the goodness of the target DGM.

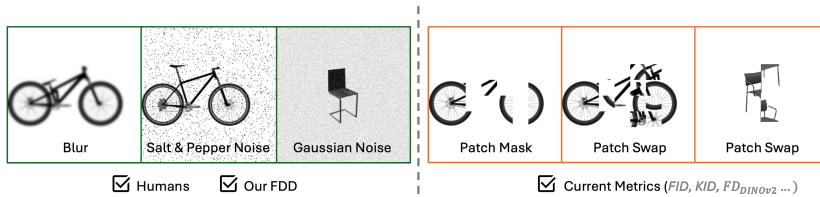


Fig. 1: From which side (*left or right*) are the designs more plausible? Recent works observe that the SOTA metrics (FID, KID and $FD_{DINO-V2}$) do not align with human judgments.

Meanwhile, the evaluation of generated images is still an unsolved challenge among other general tasks in the DGM domain [3, 4, 35]. DGM developers [7, 24, 26] are heavily relying on the Fréchet Inception Distance (FID) [21] metric, which extracts latent features from real and generated images with an Inception-V3 [46] model pre-trained on ImageNet [11] respectively and then quantifies their difference using Fréchet Distance as the final FID score. As the primary metric in the DGM field, FID is able to measure the fidelity and diversity and present them in a single value. However, a lot of studies [6, 28, 45] disclose that FID does not always align with human evaluation and claim that this limitation is due to the reliance on the pre-trained Inception-V3 model. Hence, novel metrics are delivered by replacing the Inception-V3 model by other backbone networks, *e.g.*, Clip, [37] VQ-VAE [47] and DINOv2 [36], *etc.* According to the most recent work of Stein *et al.* [45], where they compared 17 metrics using encoders from 9 various networks, $FD_{DINO-V2}$ has the most reliable performance in terms of consistency with human judgment in their experiments.

On the other hand, recent works have pointed out that the Inception-V3 model and Inception-powered metrics perform poorly on shapes [2, 14, 16, 20]. Our work investigates this finding and observes that the state-of-the-art (SOTA) metrics generally suffer from this issue: they are sensitive to visual artifacts like noises, yet they have a high tolerance towards semantic failures, *e.g.*, part missing in a bicycle, as illustrated in Fig. 1. Besides, human experts are able to recognize the same structural representation of the observed design image regardless of minor noise and they tend to penalize the evaluation based on the implausibility of the design more, rather than the presence of visual artifacts [27, 30]. Motivated by this, our work aims to create a novel metric for generative design that is robust to visual corruption of the observed images and biased towards the design plausibility.

Finally, we propose the Fréchet Denoised Distance (FDD) by replacing the Inception-V3 model within the FID framework with a Denoising Autoencoder (DAE) [48] that has been also pre-trained on ImageNet dataset and capable of encoding images into latent features with an Inception-comparable dimension of \mathbb{R}^{2048} . The DAE is able to observe the same structural representation in the image regardless of the noisy disturbances, which can be utilized as a strong method to extract the structural feature from the noisy input. Our work com-

compares our FDD with other SOTA metrics, *e.g.*, FID, $FD_{\text{DINO-V2}}$ and Topology Distance (TD) [23] (since their results show a similar bias to our intention), based on the following experiments: (1) sensitivity test over visual artifacts and structural failures; (2) consistency test with increasing disturbances; (3) consistency test with human judgment in model ranking. As a result, our FDD has the most stable performance among all the experiments. Additionally, we visualize the “focus” of our ImageNet-trained DAE compared to the Inception-V3 model with a GradCAM [28, 43, 45] test, hereby showcasing that the DAE model has a better assessment regarding the requirements of human designers.

2 Related Work

Unlike the swift development in the field of Deep Generative Models (DGMs) [12, 17, 26], accurately ranking generative models remains an unresolved challenge [3, 4, 35]. Humans are able to give the ground-truth evaluation in assessing a limited number of generated images, but quantifying the performance of a DGM requires an automated evaluation method [45]. Overcoming the flaws of previous metrics, *e.g.*, SSIM [51], LPIPS [50] and IS [42], currently most reported evaluation methods, *e.g.*, Fréchet Inception Distance (FID) [21] and Kernel Inception Distance (KID) [5], have largely addressed the challenge of automated evaluation and are employed as the primary metric for model ranking in the field of DGM [7, 24, 26]. They leverage a two-step procedure: encode real and generated images into latent features in a lower-dimensional space with a representation extractor and then use a distance critic to quantify the difference between their features. Both FID and KID utilize the Inception-V3 [46] model pre-trained on ImageNet, which has a 2048-dimensional latent space. Regarding the measurement of latent distance: FID fits the Inception features from real and generated images into a multivariate Gaussian before computing the Fréchet Distance (also known as the Wasserstein-2 distance) between them; whereas KID [5] uses the squared Maximum Mean Discrepancy (MMD) [18] with a polynomial kernel [4].

Concerns about the over-reliance on the Inception-V3 model have been raised and researchers claim that an ImageNet [11] classifier like the Inception-V3 model brings a significant bias to the evaluation with FID [35, 36]; Furthermore, FID is proved to be vulnerable to manipulation [28], especially when there exists a significant domain discrepancy between the data set of interest such as BIKED [39] and ImageNet [11]. Consequently, the results measured by FID often show a poor correlation with human judgments. Similarly, KID [5] encounters the same issue as it also leverages the pre-trained Inception-V3 model. Recent studies have introduced autoencoder-based metrics for evaluation purposes: for instance, Maiorca *et al.* [34] proposed the Fréchet Motion Distance for evaluation of synthesized human motions with the underlying motivation that an autoencoder can be trained and used on the specific data, *i.e.*, human motions; Buzuti *et al.* [8] leveraged the VQ-VAE [47] and showed that their unsupervised model-based metric outperforms FID in terms of consistency with increasing disturbance when evaluating on human and animal faces, *i.e.*, CelebA

HQ [33], FFHQ [26], and AFHQ [10]. However, their study [8] did not perform crossover comparisons among various types of disturbance. Therefore it remains uncertain which kind of image disturbance has the most contribution to the evaluation result. Most recently, in order to find a perceptual representation space superior to the inception manifold, Stein *et al.* [45] studied 17 metrics with 9 different encoders (*e.g.*, CLIP [37], SwAV [9] and DINOv2 [36]). Their finding concludes that $\text{FD}_{\text{DINO-V2}}$ [45] demonstrates the most reliable performance over various perspectives, *e.g.*, fidelity, diversity, rarity, and memorization of generative models. Previous works [2, 16, 20] shed light on the role played by the image attributes, *e.g.*, edges, shapes, textures, and colors in various computer vision tasks, *e.g.*, classification and segmentation. They revealed the limitation of ImageNet-trained CNNs in recognizing shapes. This flaw may explain the inconsistency of CNN-based metrics with human judgments when evaluating design images, where human experts prefer to use shape information for assessment [27, 30].

In other studies, new metrics have been proposed to evaluate fidelity and diversity, including density and coverage [35], as well as precision and recall [29, 41]. Others Horak *et al.* [23] have introduced a novel methodology, by examining the topological characteristics of the latent manifolds, hereby proposing the Topology Distance (TD) as a complementary metric to FID.

3 Method

Considering the preference of human designers, the metric required by design generation should “deprioritize” the visual artifacts and instead focus on evaluating the underlying shape. To achieve this, we come to the idea of replacing the Inception-V3 [46] model with the encoder of a trained Denoising Autoencoder (DAE) [48]. Following this, our work introduces the Fréchet Denoised Distance (FDD).

3.1 Preliminaries

Fréchet Inception Distance (FID) The FID leverages the ImageNet-trained Inception-V3 model without its last fully connected layer. Hereby, it provides a lower-dimensional latent space. Real images \mathbf{x} and generated images \mathbf{x}' are embedded into the Inception features $\mathbf{w} \in \mathbb{R}^{2048}$ and $\mathbf{w}' \in \mathbb{R}^{2048}$, respectively, and then separately fit into two multivariate Gaussian distributions, with $(\mu_{\mathbf{w}}, \Sigma_{\mathbf{w}})$ and $(\mu_{\mathbf{w}'}, \Sigma_{\mathbf{w}'})$ denoting the means and covariances thereof. The difference between the two latent manifolds will be quantified with Fréchet Distance with:

$$\text{FD} = \|\mu_{\mathbf{w}} - \mu_{\mathbf{w}'}\|_2^2 + \text{Tr}(\Sigma_{\mathbf{w}} + \Sigma_{\mathbf{w}'} - 2(\Sigma_{\mathbf{w}}\Sigma_{\mathbf{w}'})^{\frac{1}{2}}), \quad (1)$$

where $\text{Tr}(\cdot)$ computes the trace of a matrix.

Denoising Autoencoder (DAE) The DAE [48] is able to observe the same structural representation in the image regardless of the noisy disturbances, which

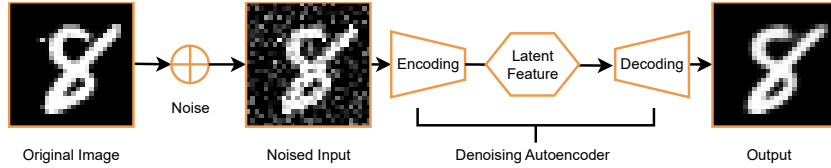


Fig. 2: Denoising Autoencoder. DAE is robust against partial visual disturbance and is trained to restore noisy images back to their original state. The *output* image is obtained by implementing a DAE trained on MNIST [31] on the *Noised Input*.

demonstrates its robustness in assessing structural plausibility. The architecture of DAE is based on an expansion of the fundamental autoencoder model, consisting of two components: an encoder ($E_\theta: \mathbf{x} \rightarrow \mathbf{w}$) and a decoder ($D_\theta: \mathbf{w} \rightarrow \mathbf{x}$). In the training phase, source images $\mathbf{x} \in \mathbb{R}^{w \times h \times c}$ are corrupted with Gaussian noises $\mathbf{x}_\eta = \mathbf{x} + \eta$, where $\eta \sim \mathcal{N}(\mathbf{0}, \sigma^2 \cdot \mathbf{I})$ and σ refers to the noise scale. The encoder (E_θ) embeds the noised image \mathbf{x}_η into its lower-dimension latent representation $\mathbf{w} = E_\theta(\mathbf{x}_\eta)$, then the decoder restores the latent representation back into pixel-based image space $\hat{\mathbf{x}} = D_\theta(\mathbf{w}) = D_\theta \circ E_\theta(\mathbf{x}_\eta)$. The network is trained using the following loss function:

$$\min_{E_\theta, D_\theta} \Delta(\mathbf{x}, \hat{\mathbf{x}}) = \frac{1}{n} \sum_{i=1}^n (\mathbf{x}_i - \hat{\mathbf{x}}_i)^2 = \frac{1}{n} \sum_{i=1}^n (\mathbf{x}_i - D_\theta \circ E_\theta(\mathbf{x}_i + \eta))^2, \quad (2)$$

where n is the batch size.

3.2 Fréchet Denoised Distance (FDD)

We implement the encoder $E_\theta(\mathbf{x}_\eta)$ of the Denoising Autoencoder (DAE) as the feature extractor. First, we design a DAE architecture (refer to Sec. 4.2 for more information on this architecture) and train it on the ImageNet [11] dataset with input shape of $299 \times 299 \times 3$. Second, similarly to the procedure of FID, we embed a certain number K of real images \mathbf{x} and generated images \mathbf{x}' into the latent features $\mathbf{w} \in \mathbb{R}^{2048}$ and $\mathbf{w}' \in \mathbb{R}^{2048}$, respectively. Note that the image is preprocessed into a shape of $299 \times 299 \times 3$ regardless of the original shape and color. Next, we follow the procedure of the Fréchet distance, introduced in Sec. 3.1, to quantify the difference between the two manifolds \mathbf{w} and \mathbf{w}' . Hereby, we design the Fréchet Denoised Distance (FDD), illustrated with an explanatory diagram in Fig. 3.

By simulating the design processes of KID [5] and TD [23] and replacing the distance measures with Maximum Mean Discrepancy (MMD) and Topology Distance (TD), we separately deliver Kernel Denoised Distance (KDD) and Topology Denoised Distance (TDD). The work of [16] trains a ResNet-50 [19] model on an alternative dataset of ImageNet, *i.e.*, Stylized-ImageNet, and hereby successfully develops a shape-biased classifier. Inspired by this proposal, we additionally train a DAE model from scratch on the BIKED [39] dataset. The DAE model trained on BIKED images has an input shape of $256 \times 256 \times 1$ and a smaller latent space with dimension $D_w = 64$. Hereby, we design an FDD (BIKED) metric, which will be evaluated on BIKED images as detailed in Sec. 4.

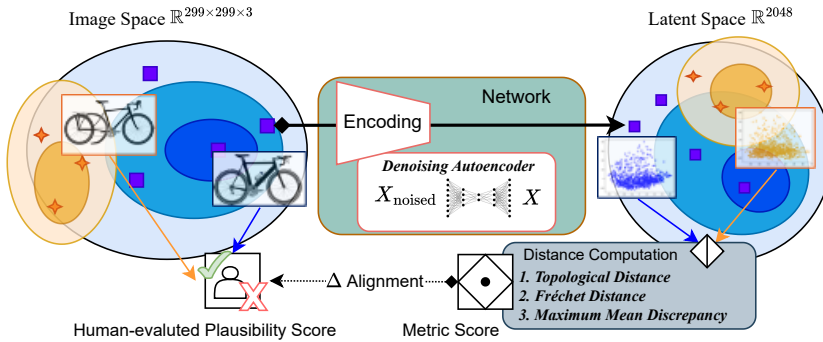


Fig. 3: Plausibility evaluation using Fréchet Denoised Distance. *Blue area and squares* visualizing real images and their latent features; *Orange area and stars* illustrating generated images and their latent features.

4 Experiments

To evaluate the design plausibility of generated images, a useful metric should satisfy the following conditions: (1) bias toward design structure, (2) consistency with increasing disturbances, and (3) alignment with human judgment. Hence, we leverage correspondingly three experiments: sensitivity test, consistency test with increasing disturbances, and model ranking, over the the SOTA metrics and our metrics (see Tab. 1 for more detailed information). Note that in our work, the TD metric refers to TD-Inception [23] unless otherwise explained.

4.1 Datasets

We select a variety of datasets covering different aspects. For a fair comparison with the FID, we train the DAE on the ImageNet [11] dataset, ensuring that the learned feature manifold is similar to the one of the Inception-V3 model. Our comparative analysis and tests also incorporate two structured datasets, BIKED [39] and Seeing3DChairs [1], to address the interests of human designers. Additionally, we incorporate the color-channeled FFHQ [26] dataset into our metric testing to confirm the metric’s adaptability to general image generation tasks. Below we list the details of the implemented datasets:

ImageNet We employ a subset of the ImageNet [11] dataset of 50 000 samples with dimension $299 \times 299 \times 3$, properly chosen to cover a wide range of 1k classes. The dataset is divided into 45 000 training samples and 5 000 test samples and is implemented for training the DAE model.

BIKED The BIKED [39] dataset is a compilation of 4 512 unique bicycle designs, contributed by various designers. The images are preprocessed into gray-scaled images with a resolution of 256×256 . We have allocated 1 000 images for testing, 100 images for validation, and the remaining 3 412 images for training purposes.

Table 1: A list of candidate performance metrics for measuring design plausibility

| Metric | Backbone Model | Input Dimension | Feature Dimension | Training Dataset | Distance Measures |
|----------------------------|---------------------------|---------------------------|----------------------|---------------------|--------------------------|
| FID [21] | Inception-V3 [46] | $299 \times 299 \times 3$ | 2048 | ImageNet [11] | Fréchet Distance |
| KID [5] | | | | | Maximum Mean Discrepancy |
| $FD_{\text{DINO-V2}}$ [45] | DINOv2 [36], ViT [13] | $224 \times 224 \times 3$ | 1024 | LVD-142M [45] | Fréchet Distance |
| TD-Inception [23] | Inception-V3 [46] | $299 \times 299 \times 3$ | 2048 | ImageNet [11] | Topology Distance |
| TD-ResNet [23] | ResNet18 [19] | $224 \times 224 \times 3$ | 512 | Fashion-MNIST [49] | |
| FDD | | | | | Fréchet Distance |
| KDD | Denosing Autoencoder [48] | $299 \times 299 \times 3$ | 2048 | ImageNet [11] | Maximum Mean Discrepancy |
| TDD | | | | | Topology Distance |
| FDD (·) | Denosing Autoencoder [48] | $256 \times 256 \times 3$ | 64 | Target Dataset | Fréchet Distance |

Seeing3DChairs For our study, we also employ the Seeing3DChairs [1] dataset of 1 477 chair designs. For each chair design, there exists a set of images sampled from 62 consecutive viewpoints. We focus on the chair images with viewpoint numbers between 017-021. Hereby, we collect 6 970 samples, from which 100 images are utilized for validation, 1 000 are used for test and rest serve as training data.

Flickr-Faces-HQ (FFHQ) Our study incorporates a subset of the Flickr-Faces-HQ (FFHQ) [26] dataset, which contains over 70 000 high-resolution color images of human faces. Specifically, we select 1 000 samples from the FFHQ subset with a resolution of $256 \times 256 \times 3$.

4.2 Experimental Settings

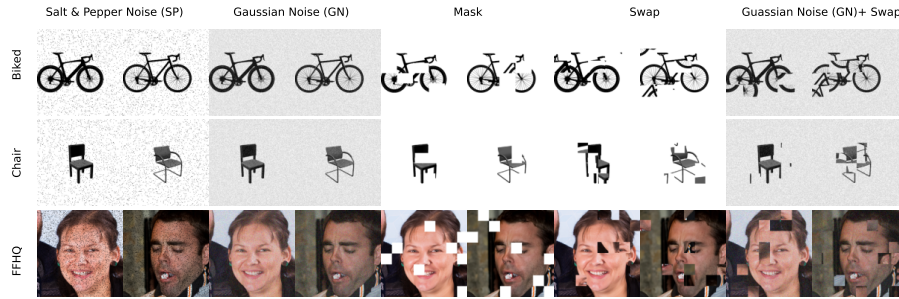
For the reproducibility of our work, this section documents all the essential details regarding the development of our FDD metric and the experimental setups. To justify the setting choices, we aim to align our DAE model’s architecture with that of the Inception-V3 model, particularly in terms of input shape and latent dimension. The model architecture and training settings describe the DAE trained on ImageNet, whereas the configurations of the DAE trained on BIKED are correspondingly adjusted as shown in Tab. 1.

Model Architecture Our approach employs a DAE comprising 5 convolution layers across both the encoder and the decoder. Here, the feature dimensions for the convolutional layers in the encoder are arranged in the following sequence [32, 64, 128, 256, 512]. For the decoder, these dimensions are applied in reverse order. Each layer employs a 3×3 kernel shape, a stride of 2, padding of 1, and the Rectified Linear Unit (ReLU) as the activation function, aligning with the Inception-V3 model. The last activation layer of the decoder uses a **Tanh** function to adjust the outputs to a pixel range of $[-1, 1]$. In alignment with the configuration parameters of the Inception-V3 model, the encoder’s input shape is specified as $299 \times 299 \times 3$, and the latent vector dimension is established at 2048.

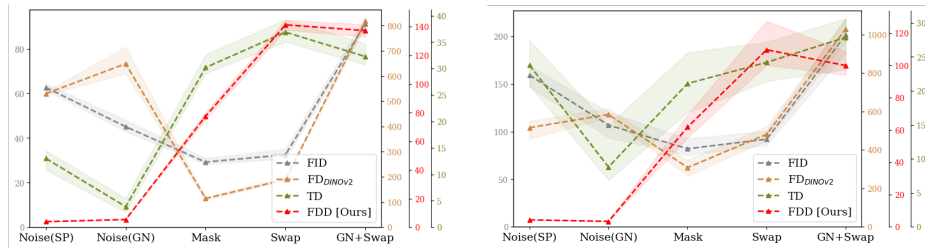
Training Settings The training process uses a subset of 50 000 images from ImageNet [11], which are rescaled to the range $[-1, 1]$. For the DAE training setup, input images are corrupted with Gaussian noise $\mathcal{N}(\mathbf{0}, \sigma^2 \cdot \mathbf{I})$ with $\sigma = 0.1$ before being fed into the encoder. We utilize the Adam Optimizer with a learning rate of $1e-3$ to train the DAE with a batch size of 128 and epochs of 1 000. The reconstruction loss is assessed by calculating the mean squared error (MSE) between the original and output images. Model performance is continuously assessed during training, and the best-performing model is chosen from the saved checkpoints for further experiments. We also implement an early stop function, where the training stops if the reconstruction loss does not reduce within 20 epochs.

Disturbance Procedures For conducting the sensitivity and consistency tests that exam metrics’ performance in dealing with various disturbances, we design the perturbation methods and their respective intensity levels based on previous studies [21, 23]. The details of the disturbances are outlined below:

- **Pepper Noise** Salt & Pepper Noise is characterized by the random conversion of image pixels to black or white. In our experiments, we specifically target pixels to turn black (*i.e.*, pepper noise), considering the prevalent white backgrounds in most design images. The proportion of image pixels altered to black, effectively setting their value to 0, is determined by a factor α within the set $[0, 0.01, 0.02, 0.03]$.
- **Gaussian Noise** We generate a random Gaussian noise in matrix form, $\boldsymbol{\eta} = \mathcal{N}(\mathbf{0}, \mathbf{I})$. Then we create noisy images \boldsymbol{x}' by adding the defined Gaussian noise to the source image \boldsymbol{x} : $\boldsymbol{x}' = (1 - \alpha)\boldsymbol{x} + \alpha\mathcal{N}(\mathbf{0}, \mathbf{I})$, where $\alpha \in [0, 0.1, 0.2, 0.3]$ refers to the intensity of the noise. The larger α is, the more intensive the disturbance of the source data is.
- **Gaussian Blur** We apply a Gaussian blur to the images using a convolution operation with a Gaussian kernel. The standard deviation of the kernel, determined by α , varies from $[0, 1, 2, 3]$, resulting in progressively more blurred images.
- **Patch Mask** For design images (BIKED and Seeing3DChairs), we evenly divide the focus area of each image (where the design object is usually located) into 16 patches. For the FFHQ-256 dataset, the entire image is segmented into 64 patches. Afterward, we randomly select a portion of patches denoted by $\alpha \in [0, 0.25, 0.5, 0.75]$ and apply a white mask to them.
- **Patch Swap** Using the same patch division approach as the Patch Mask, we randomly select a subset of patches, indicated by $\alpha \in [0, 0.25, 0.5, 0.75]$, and swap their positions pair-wisely.
- **Elastic Transformation** The image is deformed by displacing a grid of control points. Each point is shifted randomly in both the horizontal and vertical directions, typically following a Gaussian distribution to determine the displacement magnitude. The degrees of the distortion are regulated by adjusting the standard deviation of the Gaussian filter $\alpha \in [0, 4, 5, 6]$.

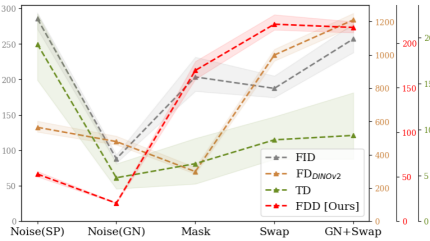


(a) Manipulated images

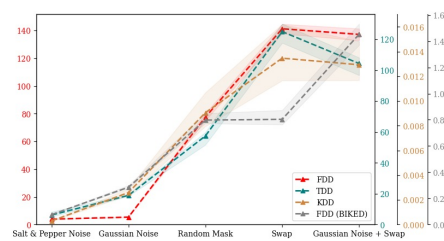


(b) Metric comparison on BIKED [39]

(c) Seeing3DChairs [1]



(d) FFHQ-256 [26]



(e) FDD Mutations on BIKED [39]

Fig. 4: Sensitivity Comparison. *Dashed lines* show means and *shaded regions* depict the measured values from the groups.

4.3 Sensitivity Test

Horak *et al.* [23] conducted the comparison of FID, KID, and TD on CelebA images [33] by corrupting the source images through the introduction of pixel noise, patch masking, and patch swapping. The study showed that the disturbance pixel noise significantly influences the evaluation results measured by FID and KID, while the innovative metric TD correlates more with human expert assessments. Motivated by this finding, we regard TD as a competitive candidate and conduct a re-run of the sensitivity test including our FDD metric. The aim of the sensitivity test is to cross-compare the metric performance in dealing with various disturbances.

This test involves three datasets: BIKED [39], Seeing3DChairs [1] and FFHQ-256 [26]. For each dataset, we shuffle and split the samples into $n = 10$ groups, number of samples in each group varies from the dataset: $K = 300$ (BIKED), $K = 100$ (Seeing3DChairs) and $K = 100$ (FFHQ-256). We introduce five types

of disturbances into source images and create five corrupted counterparts, *e.g.*, pepper noise, Gaussian noise, patch mask, patch swap and a mix of Gaussian noise and patch swap. The introduced disturbances adhere to a rule where visual artifacts, such as pepper noise and Gaussian noise, are intentionally kept at levels that do not significantly impact the recognition of the design. On the other hand, structural failures, such as patch masking and patch swapping, lead to designs that are unrecognizable and consequently receive lower human evaluation scores compared to visual artifacts. We choose one level from each disturbance described in Sec. 4.2: $\alpha_{\text{pepper noise}} = 0.01$, $\alpha_{\text{Gaussian noise}} = 0.01$, $\alpha_{\text{patch mask}} = 0.25$, and $\alpha_{\text{patch swap}} = 0.25$. Next, we measure the distance between each one of these corrupted image sets and the original image set, using FID, $\text{FD}_{\text{DINO-V2}}$, TD, and our FDD. Since they are measures of distance quantifying the dissimilarity between observed images and source images, a smaller value indicates greater similarity to the source data. On BIKED images, we additionally test the sensitivity performance of other mutation metrics, KDD, TDD, and FDD (BIKED).

Despite the presence of noise, a human designer can still recognize the underlying structure in a design. However, designs that are patch-masked or switched become less usable. Thus, we designed the sensitivity test with the anticipation that an appropriate metric for the design generation evaluation task should progressively demonstrate deteriorating scores from visual artifacts to structural deficiencies. Additionally, to prove the importance of structural integrity in the evaluation process, we expect that the score for a mixed disturbance of Gaussian noise and patch swap will be comparable to that of solely patch swap disturbance, thus remaining independent from the added visual artifacts.

We plot several examples of disturbed images and record the measured results in Fig. 4. As expected, FID [21] and $\text{FD}_{\text{DINO-V2}}$ [45] show a great bias towards visual artifacts, with notably higher distance assigned to pepper and Gaussian noised images compared to those with patch mask and patch swap. In contrast to FID and $\text{FD}_{\text{DINO-V2}}$, TD and our FDD provide a distinct evaluation perspective by detecting structural faults and imposing penalties accordingly. One unanticipated result was that TD exhibits a poor performance with regard to pepper noises as illustrated in Fig. 4c and Fig. 4d. Furthermore, as the sample size decreases within each group from 300 (BIKED [39]) to 100 (for Seeing3DChairs [1] and FFHQ [26]), TD shows a significant increase in standard deviation across

| | FID | $\text{FD}_{\text{DINOv2}}$ | TD | FDD | KDD | TDD | FDD† |
|-----------------------------|-------|-----------------------------|-------|-------|-------|------|------|
| FID | 1.0 | 0.87 | -0.03 | 0.12 | 0.03 | 0.05 | 0.39 |
| $\text{FD}_{\text{DINOv2}}$ | 0.87 | 1.0 | -0.42 | -0.18 | -0.22 | -0.2 | 0.13 |
| TD | -0.03 | -0.42 | 1.0 | 0.93 | 0.9 | 0.89 | 0.77 |
| FDD | -0.12 | -0.18 | 0.93 | 1.0 | 0.98 | 0.98 | 0.88 |
| KDD | -0.03 | -0.22 | 0.9 | 0.98 | 1.0 | 0.96 | 0.88 |
| TDD | -0.05 | -0.2 | 0.89 | 0.98 | 0.96 | 1.0 | 0.81 |
| FDD† | -0.39 | 0.13 | 0.77 | 0.88 | 0.88 | 0.81 | 1.0 |

Pearson correlation

Fig. 5: Correlation test. Pearson correlation of metrics over all distances measured for the sensitivity test with the BIKED [39] dataset. FDD† refers to FDD pre-trained on the BIKED data.

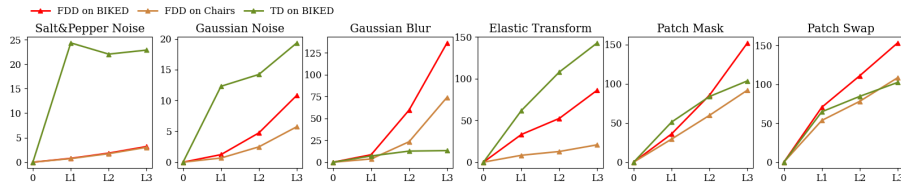


Fig. 6: Metric comparison with increasing disturbances

10-times implementations. Interestingly, our FDD shows more stability among various noises and gives significantly worse scores to images with structural failures.

Furthermore, we extend our metric by incorporating concepts from existing works such as KID [5], TD [23] and training the network on structural images [16]. This adaption yields new evaluation metrics denoted as KDD, TDD, and FDD (BIKED), respectively. Later on, we subject these metrics to the sensitivity test and present the results in Fig. 4e. Our analysis reveals that FDD exhibits the most consistent performance across various criteria: the most stable result across different groups and excellence in distinguishing between visual and structural disturbances.

Finally, we calculate the Pearson correlation coefficients pair-wisely among all candidate metrics, by taking the measured values from Fig. 4b, and record the outcome in the table Fig. 5. Notably, the result reveals two categories among the metrics: FID and $FD_{DINO-V2}$ are grouped together, while TD and our designed metrics demonstrate a stronger correlation with each other. This is a promising finding since TD’s main perspective is the topology and geometric behavior of the latent space, hereby we argue that the latent space of our DAE maintains the topological properties of the image space well and can be captured by Fréchet Distance.

4.4 Consistency with Increasing Disturbances

In this section, we test the consistency of the FDD metric in response to escalating levels of disturbances outlined in Sec. 4.2. As a fundamental requirement, a performance metric should be able to accurately detect and respond to worsened image quality, including visual fidelity and structural plausibility. We start by adding various disturbances to a subset comprising $K = 1000$ images sourced from the BIKED [39] and Seeing3DChairs [1] datasets, respectively. Afterwards, we report the scores in Fig. 6 and demonstrate the consistent performance of the proposed FDD metric. While FID has been noted to exhibit inconsistency in detecting the disturbance level induced by salt and pepper as documented in Heusel *et al.* [21], our FDD successfully measures the levels of various deformations, spanning from visual to structural distortions.

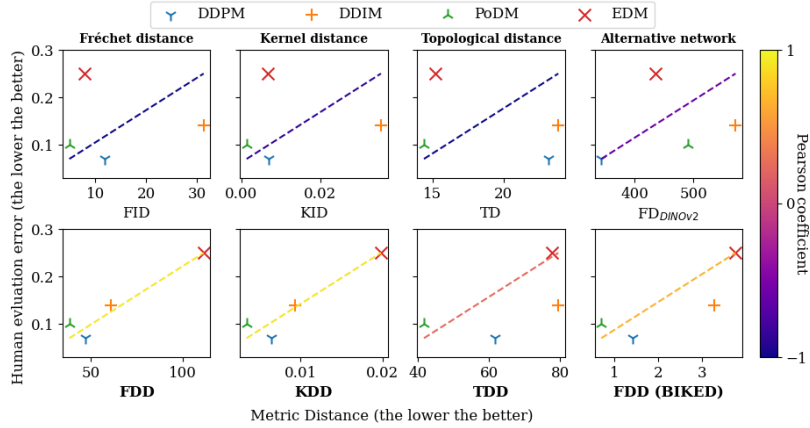


Fig. 7: Metrics comparison in the task of model ranking. We color-code the *diagonal lines* after the measured Pearson correlation coefficient between metric results and human judgments, *bright yellow* refers to a strong positive correlation between metric distances and human judgments.

4.5 Model Ranking

In the model ranking, we employ the following five generative models, DDPM [22], DDIM [44], EDM [25] and PoDM [14], with the consideration that the models executed in model ranking should exhibit significant differences in visual quality and structural plausibility. These models are then trained on BIKED images with a resolution of 256×256 . We generate 5k images from each model and manually evaluate them into plausible designs and implausible designs. We denote the ratio of implausible bicycle designs as human evaluation error, the lower the better, which serves as the “ground truth” in this model ranking experiment.

Meanwhile, we apply the candidate metrics, including FID, KID, $FD_{DINO-V2}$, TD, FDD, and its variants, to compute the distance between generated images and source images for each model, with 1k images in each group. Subsequently, the distances measured and human error rates are visualized in Fig. 7. Note that the proximity of the plotted points (measured distances, human evaluation error) to the diagonal line signifies the consistency of the metric with human evaluation. Particularly, the expected behavior is seen in the FDD, KDD, and FDD (BIKED) measurements, which are highly associated and yield the same consistent ranking. This observation aligns with the notion proposed by [45], whereby provided a good encoder is chosen, all these metrics provide sensible ways of quantifying distances between probability distributions. On the other hand, the absence of a significant link between the SOTA metrics and human evaluation suggests a deficiency of these most reported metrics in evaluating structural design images. In Fig. 8, we plot the generated bicycles for qualitative evaluation of our FDD metric. EDM achieves the best FID of 7.84, but the generated bicycles contain a large portion of implausible designs; DDIM is unfairly

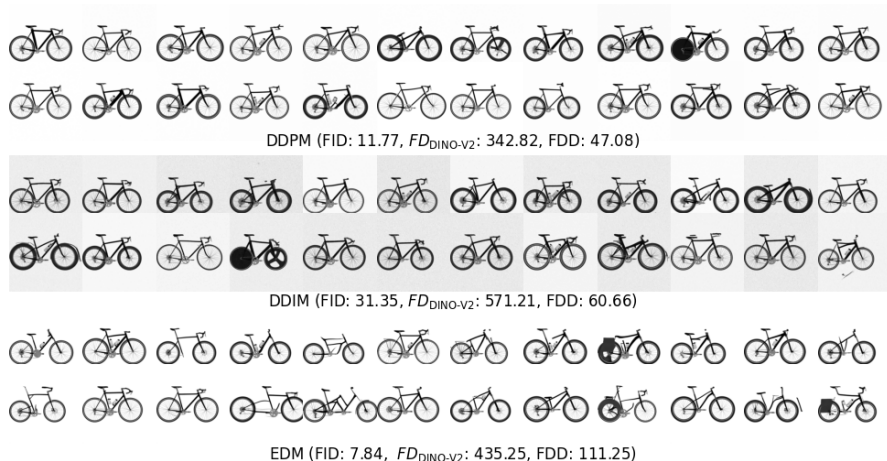


Fig. 8: Qualitative evaluation of generated bicycle designs. DDPM and DDIM yield structurally more plausible results than EDM, but FID and $FD_{\text{DINO-V2}}$ fail to agree with human judgments, whereas our FDD ranks the models with the perspective of structural plausibility.

penalized (with a FID of 31.35), even though the results are significantly more plausible than those from EDM. Here, our FDD is able to rank the models more accurately.

4.6 Grad-CAM visualization

The Grad-CAM [43] is designed to visualize the focus on the input image as perceived by the classifier/segmentation model up to the last fully connected layer. In our work, we use the Grad-CAM visualization to compare the observation fields of the FID and FDD metrics. We adopt the work introduced by [32, 43] and compute the attention maps by back-propagating the corresponding FID and FDD values to the last convolutional layer of the Inception-V3 model (*i.e.*, *Mixed 7c.branch.pool*) and the one of DAE (*i.e.*, *encoder 8*), respectively. The Grad-CAM generates a heatmap of reduced dimensions (*e.g.*, 10×10 for DAE) which is then upsampled to match the dimensions of the original image for intuitive visual comparison. The heatmaps (seen in Fig. 9) visualize the area observed by the corresponding metric in the BIKED [39] images, *i.e.*, where the metric “looks at” when it calculates the distance. The focus of the Inception-V3 model is simply the area around the center of the main object, often mismatching the object’s shape and borders. To better understand this observation, note that the ImageNet dataset has a sparse representation of bike categories, and as a result, the highlighted area in the heatmap reflects the model’s top-1 class prediction features. As explained in previous works [28, 45], this phenomenon is caused by the model’s classification training across 1000 classes. Consequently, it prioritizes detecting the object’s presence rather than its structure. On the other hand, the important features, according to the DAE, are typically parts of the bike’s structure. DAE generates an intensive attention map with positive

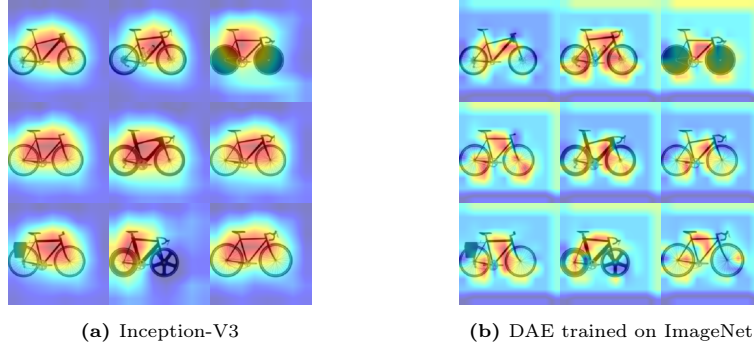


Fig. 9: Heatmaps illustrating the perception of the Fréchet distance. The focus of an encoder can be demonstrated by both *bright red* and *deep blue*.

and negative gradients surrounding the bicycle’s structure, which efficiently separates the bicycle design from the empty background and hereby enhancing the model’s ability to comprehend the complex details of the bicycle’s shape.

5 Conclusion

In this work, we approached the field of evaluating generated design images and proposed a structure-biased metric Fréchet Denoised Distance (FDD) by replacing the Inception-V3 model in the FID metric with a Denoising Autoencoder, trained on the same dataset, *i.e.*, ImageNet, and with the same 2048-dimensional latent space. Through a series of experiments, including sensitivity test for various types of disturbance, consistency test with increasing disturbances, and alignment test with human judgment in model ranking, we found FDD to fulfill the quality requirements for serving as a metric and outperform other metrics, *e.g.*, FID, $FD_{DINO-V2}$ and TD, on design images such as BIKED and Seeing3DChairs, as well as real-world images such as human faces from FFHQ. We explained the effectiveness of FDD with a Grad-CAM visualization, where the DAE is able to “focus” on the design structure of the observed shape.

Limitation and Future Work FDD has a low priority towards visual artifacts, which may become problematic in contexts where the visual quality is critical. Yet, our experiments demonstrated that when there is no major structural failure, it is still capable of observing visual artifacts. In addition, we believe that this novel insight may also be useful in guiding DGMs to generate more reliable, plausible designs, which is of great potential to be further investigated in future work. Finally, while our research on FDD mainly focused on image space, considering the advanced study of 3D Diffusion modeling (adding noise to 3D data) and the use of Autoencoders to process 3D data, we believe that FDD can also assess 3D-DGMs.

References

1. Aubry, M., Maturana, D., Efros, A.A., Russell, B.C., Sivic, J.: Seeing 3d chairs: Exemplar part-based 2d-3d alignment using a large dataset of cad models. In: 2014 IEEE CVPR. pp. 3762–3769 (2014). <https://doi.org/10.1109/CVPR.2014.487>
2. Baker, N., Lu, H., Erlikhman, G., Kellman, P.J.: Deep convolutional networks do not classify based on global object shape. *PLoS Computational Biology* **14** (2018), <https://api.semanticscholar.org/CorpusID:54476941>
3. Barratt, S.T., Sharma, R.: A note on the inception score. *ArXiv abs/1801.01973* (2018), <https://api.semanticscholar.org/CorpusID:38384342>
4. Betzalel, E., Penso, C., Navon, A., Fetaya, E.: A study on the evaluation of generative models. *CoRR abs/2206.10935* (2022). <https://doi.org/10.48550/ARXIV.2206.10935>, <https://doi.org/10.48550/arXiv.2206.10935>
5. Binkowski, M., Sutherland, D.J., Arbel, M., Gretton, A.: Demystifying MMD gans. In: 6th International Conference on Learning Representations, ICLR 2018, Vancouver, BC, Canada, April 30 - May 3, 2018, Conference Track Proceedings. OpenReview.net (2018), <https://openreview.net/forum?id=r1lU0zWCW>
6. Borji, A.: Pros and cons of gan evaluation measures: New developments. *Computer Vision and Image Understanding* **215**, 103329 (2022). <https://doi.org/https://doi.org/10.1016/j.cviu.2021.103329>, <https://www.sciencedirect.com/science/article/pii/S1077314221001685>
7. Brock, A., Donahue, J., Simonyan, K.: Large scale gan training for high fidelity natural image synthesis. *ArXiv abs/1809.11096* (2018), <https://api.semanticscholar.org/CorpusID:52889459>
8. Buzuti, L.F., Thomaz, C.E.: Fréchet autoencoder distance: A new approach for evaluation of generative adversarial networks. *Computer Vision and Image Understanding* **235**, 103768 (2023)
9. Caron, M., Misra, I., Mairal, J., Goyal, P., Bojanowski, P., Joulin, A.: Unsupervised learning of visual features by contrasting cluster assignments. In: Proceedings of the 34th International Conference on Neural Information Processing Systems. NIPS'20, Curran Associates Inc., Red Hook, NY, USA (2020)
10. Choi, Y., Uh, Y., Yoo, J., Ha, J.W.: Stargan v2: Diverse image synthesis for multiple domains. In: 2020 IEEE/CVF Conference on Computer Vision and Pattern Recognition (CVPR). pp. 8185–8194 (2020). <https://doi.org/10.1109/CVPR42600.2020.00821>
11. Deng, J., Dong, W., Socher, R., Li, L.J., Li, K., Fei-Fei, L.: Imagenet: A large-scale hierarchical image database. In: *Computer Vision and Pattern Recognition, 2009. CVPR 2009. IEEE Conference on*. pp. 248–255. IEEE (2009), <https://ieeexplore.ieee.org/abstract/document/5206848/>
12. Dhariwal, P., Nichol, A.Q.: Diffusion models beat GANs on image synthesis. In: Beygelzimer, A., Dauphin, Y., Liang, P., Vaughan, J.W. (eds.) *Advances in Neural Information Processing Systems* (2021), <https://openreview.net/forum?id=AAWuCvzaVt>
13. Dosovitskiy, A., Beyer, L., Kolesnikov, A., Weissenborn, D., Zhai, X., Unterthiner, T., Dehghani, M., Minderer, M., Heigold, G., Gelly, S., et al.: An image is worth 16x16 words: Transformers for image recognition at scale. *arXiv preprint arXiv:2010.11929* (2020)
14. Fan, J., Vuaille, L., Bäck, T., Wang, H.: On the noise scheduling for generating plausible designs with diffusion models (2023)

15. Fan, J., Vuaille, L., Wang, H., Bäck, T.: Adversarial latent autoencoder with self-attention for structural image synthesis. arXiv preprint arXiv:2307.10166 (2023)
16. Geirhos, R., Rubisch, P., Michaelis, C., Bethge, M., Wichmann, F., Brendel, W.: Imagenet-trained cnns are biased towards texture; increasing shape bias improves accuracy and robustness. ArXiv **abs/1811.12231** (2018), <https://api.semanticscholar.org/CorpusID:54101493>
17. Goodfellow, I., Pouget-Abadie, J., Mirza, M., Xu, B., Warde-Farley, D., Ozair, S., Courville, A., Bengio, Y.: Generative adversarial nets. In: Advances in neural information processing systems. pp. 2672–2680 (2014), <http://papers.nips.cc/paper/5423-generative-adversarial-nets.pdf>
18. Gretton, A., Borgwardt, K.M., Rasch, M.J., Schölkopf, B., Smola, A.: A kernel two-sample test. The Journal of Machine Learning Research **13**(1), 723–773 (2012)
19. He, K., Zhang, X., Ren, S., Sun, J.: Deep residual learning for image recognition. In: 2016 IEEE Conference on Computer Vision and Pattern Recognition (CVPR). pp. 770–778 (2016). <https://doi.org/10.1109/CVPR.2016.90>
20. Hermann, K.L., Chen, T., Kornblith, S.: The origins and prevalence of texture bias in convolutional neural networks. arXiv: Computer Vision and Pattern Recognition (2019), <https://api.semanticscholar.org/CorpusID:220266152>
21. Heusel, M., Ramsauer, H., Unterthiner, T., Nessler, B., Hochreiter, S.: Gans trained by a two time-scale update rule converge to a local nash equilibrium. Advances in Neural Information Processing Systems 30 (NIPS 2017) (2018)
22. Ho, J., Jain, A., Abbeel, P.: Denoising diffusion probabilistic models. arXiv preprint arxiv:2006.11239 (2020)
23. Horak, D., Yu, S., Khorshidi, G.S.: Topology distance: A topology-based approach for evaluating generative adversarial networks. In: Thirty-Fifth AAAI Conference on Artificial Intelligence, AAAI 2021, Thirty-Third Conference on Innovative Applications of Artificial Intelligence, IAAI 2021, The Eleventh Symposium on Educational Advances in Artificial Intelligence, EAAI 2021, Virtual Event, February 2-9, 2021. pp. 7721–7728. AAAI Press (2021). <https://doi.org/10.1609/AAAI.V35I9.16943>, <https://doi.org/10.1609/aaai.v35i9.16943>
24. Karras, T., Aila, T., Laine, S., Lehtinen, J.: Progressive growing of gans for improved quality, stability, and variation. ArXiv **abs/1710.10196** (2017), <https://api.semanticscholar.org/CorpusID:3568073>
25. Karras, T., Aittala, M., Aila, T., Laine, S.: Elucidating the design space of diffusion-based generative models. Advances in Neural Information Processing Systems **35**, 26565–26577 (2022)
26. Karras, T., Laine, S., Aila, T.: A style-based generator architecture for generative adversarial networks. In: Proceedings of the IEEE/CVF conference on computer vision and pattern recognition. pp. 4401–4410 (2019)
27. Kucker, S.C., Samuelson, L.K., Perry, L.K., Yoshida, H., Colunga, E., Lorenz, M.G., Smith, L.B.: Reproducibility and a unifying explanation: Lessons from the shape bias. Infant behavior & development **54**, 156–165 (2019), <https://api.semanticscholar.org/CorpusID:53045726>
28. Kynkäänniemi, T., Karras, T., Aittala, M., Aila, T., Lehtinen, J.: The role of imagenet classes in fréchet inception distance. In: The Eleventh International Conference on Learning Representations (2023), https://openreview.net/forum?id=4oXTQ6m_ws8
29. Kynkäänniemi, T., Karras, T., Laine, S., Lehtinen, J., Aila, T.: Improved precision and recall metric for assessing generative models. In: Neural Information Processing Systems (2019), <https://api.semanticscholar.org/CorpusID:118648975>

30. Landau, B., Smith, L.B., Jones, S.S.: The importance of shape in early lexical learning. *Cognitive Development* **3**, 299–321 (1988), <https://api.semanticscholar.org/CorpusID:205117480>
31. Lecun, Y., Bottou, L., Bengio, Y., Haffner, P.: Gradient-based learning applied to document recognition. *Proceedings of the IEEE* **86**(11), 2278–2324 (1998). <https://doi.org/10.1109/5.726791>
32. Liu, W., Li, R., Zheng, M., Karanam, S., Wu, Z., Bhanu, B., Radke, R.J., Camps, O.: Towards visually explaining variational autoencoders. In: *Proceedings of the IEEE/CVF Conference on Computer Vision and Pattern Recognition*. pp. 8642–8651 (2020)
33. Liu, Z., Luo, P., Wang, X., Tang, X.: Deep learning face attributes in the wild. In: *Proceedings of the IEEE international conference on computer vision*. pp. 3730–3738 (2015)
34. Maiorca, A., Yoon, Y., Dutoit, T.: Evaluating the quality of a synthesized motion with the fréchet motion distance. In: *ACM SIGGRAPH 2022 Posters. SIGGRAPH '22*, Association for Computing Machinery, New York, NY, USA (2022). <https://doi.org/10.1145/3532719.3543228>, <https://doi.org/10.1145/3532719.3543228>
35. Naeem, M.F., Oh, S.J., Uh, Y., Choi, Y., Yoo, J.: Reliable fidelity and diversity metrics for generative models. In: III, H.D., Singh, A. (eds.) *Proceedings of the 37th International Conference on Machine Learning. Proceedings of Machine Learning Research*, vol. 119, pp. 7176–7185. PMLR (13–18 Jul 2020), <https://proceedings.mlr.press/v119/naeem20a.html>
36. Oquab, M., Darcet, T., Moutakanni, T., Vo, H.V., Szafraniec, M., Khalidov, V., Fernandez, P., HAZIZA, D., Massa, F., El-Nouby, A., Assran, M., Ballas, N., Galuba, W., Howes, R., Huang, P.Y., Li, S.W., Misra, I., Rabbat, M., Sharma, V., Synnaeve, G., Xu, H., Jegou, H., Mairal, J., Labatut, P., Joulin, A., Bojanowski, P.: DINOv2: Learning robust visual features without supervision. *Transactions on Machine Learning Research* (2024), <https://openreview.net/forum?id=a68SUt6zFt>
37. Radford, A., Kim, J.W., Hallacy, C., Ramesh, A., Goh, G., Agarwal, S., Sastry, G., Askell, A., Mishkin, P., Clark, J., Krueger, G., Sutskever, I.: Learning transferable visual models from natural language supervision. In: *International Conference on Machine Learning* (2021), <https://api.semanticscholar.org/CorpusID:231591445>
38. Radford, A., Metz, L., Chintala, S.: Unsupervised representation learning with deep convolutional generative adversarial networks. In: Bengio, Y., LeCun, Y. (eds.) *4th International Conference on Learning Representations, ICLR 2016, San Juan, Puerto Rico, May 2-4, 2016, Conference Track Proceedings* (2016), <http://arxiv.org/abs/1511.06434>
39. Regenwetter, L., Curry, B., Ahmed, F.: BIKED: A Dataset for Computational Bicycle Design With Machine Learning Benchmarks. *Journal of Mechanical Design* **144**(3) (10 2021). <https://doi.org/10.1115/1.4052585>, <https://doi.org/10.1115/1.4052585>, 031706
40. Regenwetter, L., Nobari, A.H., Ahmed, F.: Deep generative models in engineering design: A review. *Journal of Mechanical Design* **144**(7), 071704 (2022)
41. Sajjadi, M.S.M., Bachem, O., Lučić, M., Bousquet, O., Gelly, S.: Assessing generative models via precision and recall. In: *Advances in Neural Information Processing Systems (NeurIPS)* (2018)
42. Salimans, T., Goodfellow, I.J., Zaremba, W., Cheung, V., Radford, A., Chen, X.: Improved techniques for training gans. *ArXiv abs/1606.03498* (2016), <https://api.semanticscholar.org/CorpusID:1687220>

43. Selvaraju, R.R., Cogswell, M., Das, A., Vedantam, R., Parikh, D., Batra, D.: Grad-cam: Visual explanations from deep networks via gradient-based localization. In: 2017 IEEE International Conference on Computer Vision (ICCV). pp. 618–626 (2017). <https://doi.org/10.1109/ICCV.2017.74>
44. Song, J., Meng, C., Ermon, S.: Denoising diffusion implicit models. arXiv:2010.02502 (October 2020), <https://arxiv.org/abs/2010.02502>
45. Stein, G., Cresswell, J.C., Hosseinzadeh, R., Sui, Y., Ross, B.L., Villecroze, V., Liu, Z., Caterini, A.L., Taylor, J.E.T., Loaiza-Ganem, G.: Exposing flaws of generative model evaluation metrics and their unfair treatment of diffusion models. CoRR **abs/2306.04675** (2023). <https://doi.org/10.48550/ARXIV.2306.04675>, <https://doi.org/10.48550/arXiv.2306.04675>
46. Szegedy, C., Vanhoucke, V., Ioffe, S., Shlens, J., Wojna, Z.: Rethinking the inception architecture for computer vision. 2016 IEEE Conference on Computer Vision and Pattern Recognition (CVPR) pp. 2818–2826 (2015), <https://api.semanticscholar.org/CorpusID:206593880>
47. Van Den Oord, A., Vinyals, O., et al.: Neural discrete representation learning. *Advances in neural information processing systems* **30** (2017)
48. Vincent, P., Larochelle, H., Bengio, Y., Manzagol, P.A.: Extracting and composing robust features with denoising autoencoders. In: *International Conference on Machine Learning* (2008), <https://api.semanticscholar.org/CorpusID:207168299>
49. Xiao, H., Rasul, K., Vollgraf, R.: Fashion-mnist: a novel image dataset for benchmarking machine learning algorithms. *ArXiv* **abs/1708.07747** (2017), <https://api.semanticscholar.org/CorpusID:702279>
50. Zhang, R., Isola, P., Efros, A.A., Shechtman, E., Wang, O.: The unreasonable effectiveness of deep features as a perceptual metric. In: *2018 IEEE Conference on Computer Vision and Pattern Recognition, CVPR 2018, Salt Lake City, UT, USA, June 18-22, 2018*. pp. 586–595. Computer Vision Foundation / IEEE Computer Society (2018). <https://doi.org/10.1109/CVPR.2018.00068>, http://openaccess.thecvf.com/content_cvpr_2018/html/Zhang_The_Unreasonable_Effectiveness_CVPR_2018_paper.html
51. Zhou, W.: Image quality assessment: from error measurement to structural similarity. *IEEE transactions on image processing* **13**, 600–613 (2004)